Available online at www.sciencedirect.com
SCIENCE DIRECT®
Composites Science and Technology 65 (2005) 1264–1275
COMPOSITES SCIENCE AND TECHNOLOGY
www.elsevier.com/locate/compscitech

Elastic properties of three-phase composites: analytical model based on the modified shear-lag model and the method of cells

Juan Carlos Afonso *, Giorgio Ranalli

Department of Earth Sciences and Ottawa-Carleton Geoscience Centre, Carleton University, 1125 Colonel By Drive, Ottawa, Canada K1S 5B6

Received 27 July 2004; received in revised form 15 November 2004; accepted 23 December 2004
Available online 29 January 2005

Abstract

A new general model to calculate the elastic properties of three-phase composites by means of closed-form analytical solutions is presented. The model is based on a combination of the modified shear-lag model and the method of cells. It does not require detailed knowledge of the microstructure. This confers the new model several advantages over previous methodologies, and makes it able to be used to estimate elastic properties of three-phase composites having very different matrix-reinforcements configurations, including anisotropy effect by introducing the fibre aspect ratio. The versatility and accuracy of the model have been tested on several different materials, including concrete mixtures, ceramics, metallic alloys, and natural rocks. Good agreement is found between the estimated effective Young's modulus and the experimental results from the literature.

Keywords: Three-phase composites; B. modelling; C. elastic properties

1. Introduction

It has long been recognized that the mechanical, physical, and electrical properties of a material can be improved by combining particles or fibres embedded in a matrix. Two-phase materials have been exploited for decades in engineering design, and they have proved to be of great applicability and high performance. However, it has been suggested that some materials previously considered to be two-phase composites are better described in terms of a third phase [1,2]. Also, three-phase composites are becoming more important in many engineering fields, due to their unique weight-stiffness relationships [3,4]. Therefore, a model that can predict elastic properties of these materials as a function of simple macrophysical observables is desirable. Although some work has been done on this topic, it usually requires a detailed knowledge of the microstructure, semi-empirical constants, or complex numerical simulations. Simple closed-form relations to properly predict the behaviour of three-phase composites, based only on reliable macrophysical information, are lacking in the literature. In this contribution we present a simple general method to estimate the Young's modulus of three-phase composites, based on an appropriate combination of the modified shear-lag model and the method of cells. The model inputs are only the Young's moduli and volume fractions of the constituents, and anisotropy effects can be accounted for by means of the fibre aspect ratio (i.e., ratio of fibre length to fibre width). It is shown that the model's versatility allows it to be used for composites having different reinforcements-matrix geometries, as well as for natural polycrystalline/polymineralic rocks.

* Corresponding author. Tel.: +1 613 520 2600x4392; fax: +1 613 520 2569.
E-mail addresses: jcarlos@ccs.carleton.ca (J.C. Afonso), granalli@ccs.carleton.ca (G. Ranalli).

0266-3538/$ - see front matter © 2005 Elsevier Ltd. All rights reserved.
doi:10.1016/j.compscitech.2004.12.033

2. The model

2.1. Two-phase composites

The shear-lag model [5] is widely used to calculate deformational and elastic properties of discontinuous fibres in fibre-reinforced composites. Although the original model only considers the load transfer from the matrix to the fibres by means of shear stresses at the fibre–matrix interface, several modifications have been made to account for the stress transfer and failure mechanisms in fibre composites [6–9]. The unit cell used in the shear-lag model is shown in Fig. 1. It is composed of a uniform cylindrical matrix of length $2L$ and radius R, containing a discontinuous cylindrical fibre with radius r_1 and length $2l$. Fibre and matrix are coaxial. The unit cell is subject to a uniform tensile stress σ_a at its ends, where only the matrix is present. The applied stress is parallel to the fibre axis, and no sliding is allowed between the matrix and the fibre at the interface $r = r_1$. The axial stress in the fibre $\sigma_f(x)$ is considered to be independent of r.

The accuracy of the model is largely dependent on the imposed boundary conditions at the fibre end. Generally, stress boundary conditions, based on arbitrary assumptions, are predefined at the fibres ends to obtain analytical solutions from the governing equations [9–11]. However, as Hsueh [7] pointed out, these stresses cannot be predetermined, and therefore the boundary conditions are ambiguous. To avoid these difficulties, in the present work we adopt a scheme previously proposed by Nair and Kim [6] and Hsueh [7], where two fictitious fibres (made of matrix material), each with length L–l and width $r = r_1$ are added in the region between the fibre and the ends of the unit cell (dashed in Fig. 1). This approach is the only one which gives analytical solutions for the stress distribution in the matrix region beyond the limit $x = l$. The previous formulation however, is modified in this paper in order to express the final analytical solutions in a simple closed form and to extend the model from two to three-phase composites (see [12] for more details).

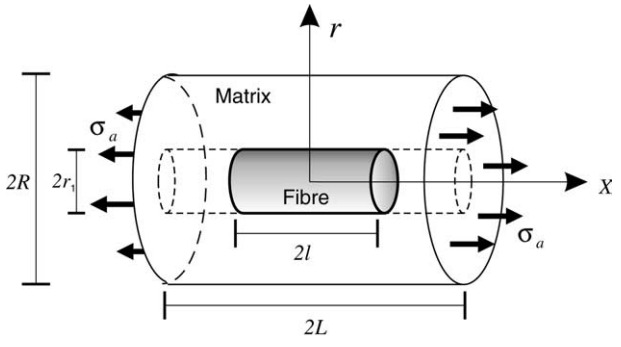

Fig. 1. Unit cell geometry and coordinate system. The shaded cylindrical region represents the fibre. Dashed cylindrical volumes represent the imaginary fibres.

Since the axial and shear stress distribution in and along the fibre are symmetric with respect to the r-axis, the equations describing these stresses can be written as (see Appendix A)

$$\sigma_f(x) = \frac{R^2 E_f \sigma_a}{S} + 2A\cosh(\beta x), \tag{1}$$

$$\tau_f(r_1, x) = -r_1 \beta A \sinh(\beta x), \tag{2}$$

where H, S and β are given in Eqs. (A.6), (A.7) and (A.9) of Appendix A. All symbols are defined in Table 1. The coefficient A needs to be determined from particular boundary conditions, and is given by Eq. (A.12) in the same appendix.

Because of the similar geometry, we can use Eqs. (1) and (2) to describe the stress transfer through and along the fictitious fibre simply by replacing the Young's modulus of the matrix for that of the fibre in Eqs. (1) and (2). However, since the stress distribution in the fictitious fibre is not symmetric with respect to the mid-point of the fibre (as it is in the real fibre), Eqs. (1) and (2) need to be rewritten as [7]

$$\sigma_{ff}(x) = \exp(\beta_f x)c_1 + \exp(-\beta_f x)c_2 + \sigma_a, \tag{3}$$

Table 1
Symbols used in this work

Symbol	Definition
L	Semi-length of the unit cell
R	Radius of the unit cell
r_1	Radius of the fibre
l	Semi-length of the fibre
σ_a	Applied tensile stress
$\sigma_f(x)$	Axial stress in the fibre
$\tau_f(r_1, x)$	Shear stress at the fibre–matrix interface
$\sigma_{ff}(x)$	Axial stress in the imaginary fibre
$\tau_{ff}(r_1, x)$	Shear stress along the imaginary fibre
E_f	Young's modulus of the fibre
E_m	Young's modulus of the matrix
v_c	Poisson's ratio of the composite
v_{f1}	Poisson's ratio of phase 1
v_{f2}	Poisson's ratio of phase 2
v_m	Poisson's ratio of the matrix
V_c	Total volume of the composite
V_{f1}	Total volume of phase 1
V_{f2}	Total volume of phase 2
V_m	Total volume of the matrix
f_{f1}	Volume fraction of phase 1
f_{f2}	Volume fraction of phase 2
f_m	Volume fraction of the matrix
f'_{f1}	Volume fraction of fibre 1 in RVE 1
f'_{m1}	Volume fraction of the matrix in RVE 1
f'_{f2}	Volume fraction of fibre 2 in RVE 2
f'_{m2}	Volume fraction of the matrix in RVE 2
E_{c1}	Young's modulus of the RVE 1
E_{c2}	Young's modulus of the RVE 2
E_{CA}	Young's modulus of RVE 1 + RVE 2 and RVE 2 + RVE 4
E_{CT}	Young's modulus of the three-phase composite

$$\tau_{\mathrm{ff}}(r_1,x) = -\frac{r_1\beta_{\mathrm{f}}}{2}[\exp(\beta_{\mathrm{f}}x)c_1 - \exp(-\beta_{\mathrm{f}}x)c_2], \tag{4}$$

where c_1 and c_2 are two new constants determined from boundary conditions, and

$$\beta_{\mathrm{f}} = \sqrt{H}. \tag{5}$$

The values of c_1 and c_2 are given in Eqs. (A.14) and (A.15) of Appendix A.

Predicted stresses in the fibre and the matrix using Eqs. (1)–(4) are given in Fig. 2. As found previously (e.g. [6,13,14]), the interfacial shear stress reaches a maximum at the fibre ends and a minimum at the mid-point. The axial stress acting at the fibre ends undergoes a significant amplification from the applied stress at the end of the unit cell (the amplification is a function of the Young's moduli contrast between the phases). This effect was also verified by finite element analysis [6,15], and challenges previous assumptions regarding the stress at the fibre ends (e.g. [14,16,17]).

The choice of a representative value for R and L in the unit cell is somehow ambiguous, since different combinations of these parameters can give the same volume for the unit cell. Different ways of doing this were proposed in the literature [9,11,17,18]. However, it has been noted that basically two end-member geometries (e.g., for long and short fibres) are sufficient to estimate the volume of the unit cell [15]. Hsueh [15] presented an ingenious approach of calculating R and L, taking into account these two different geometries, by means of the parameter p, which is a function of the fibre aspect ratio. It was found that this method gives good estimates of the Young's modulus, similar to those obtained by other common methods (e.g. Eshelby model) [15]. Here, we follow this approach for calculating representative unit cell dimensions (see Appendix B for details).

Eqs. (1)–(5) can be used to predict the Young's modulus of two-phase composites. The analysis can be done

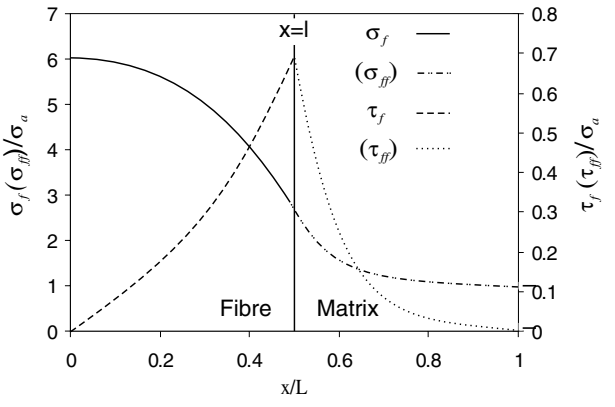

Fig. 2. Ratio of axial (σ) and shear (τ) stresses to applied axial stress (σ_{a}), vs. normalized axial distance from the midpoint of the unit cell. The solid vertical line labeled $x = l$ separates the fibre and matrix regions. $E_{\mathrm{f}}/E_{\mathrm{m}} = 10$; $\nu_{\mathrm{m}} = 0.25$; $R/r = 5$; $L/l = 2$. See text for details.

in two different ways: (a) by calculating average stresses and strains, or (b) by calculating average displacements. Both schemes give similar results, though the former is somewhat more tedious. The details of the derivation of the equations for these two methods are given in Appendix B. The Young's modulus of the two-phase composite from the shear-lag model is obtained from

$$E_{\mathrm{c}} = \frac{\sigma_{\mathrm{a}}}{\left\{\frac{\sigma_{\mathrm{a}}}{E_{\mathrm{m}}} + \left[\left(\frac{2A\sinh(\beta l)}{\beta} + \frac{lR^2E_{\mathrm{f}}\sigma_{\mathrm{a}}}{S}\right) \times \left(\frac{1}{E_{\mathrm{f}}} - \frac{1}{E_{\mathrm{m}}}\right)\frac{r_1^2}{LR^2}\right]\right\}}. \tag{6}$$

Eq. (6) is fundamentally similar to that obtained by Hsueh [15]. It should be noted that the values predicted from Eq. (6) are strictly valid at applied stresses (i.e. service loads) below the yield strength of both the matrix and the fibre. As stated above, the amplification of $\sigma_{\mathrm{f}}(r_1,l)$, acting at the fibre ends, indicates that at sufficiently high applied stresses, both shear and axial stress can reach locally the yield strength of the matrix or fibre, resulting either in plastic deformation, debonding, formation of cracks, fracture of fibres, or a combination of these phenomena. Eqs. (1)–(4) can be used together with experimental values of failure stress (strain) and Young's moduli of the phases to estimate the range of applicability of Eq. (6), and the onset of inelastic behaviour of the composite [13].

Results from Eq. (6) are compared with experimental data and finite element analysis in Fig. 3. Excellent agreement between the published data and the predicted Young's modulus of the composites was obtained in all cases. For comparison, also plotted in Fig. 3 are predictions based on the equations presented by Taya and Arsenault [17] (T&A), those obtained from the Reuss–Voigt–Hill average method [19] (R–V–H), and those from the modified shear-lag model presented by Starink and Syngellakis [9] (S&S). Table 2 lists the elastic properties of the constituent phases of the composites.

The equation used by T&A, also derived from the shear-lag model, neglects the stress intensification at the fibre ends. This equation is always found to underestimate the modulus of the composite as determined experimentally, by about 15–65%, in particular when the aspect ratio is small (see also [6,13]). On the other hand, the R–V–H model usually overestimates the modulus of the composite, the associated error being particularly significant when the matrix is relatively soft (i.e., Young's modulus of the order of 2–6 GPa), as it can be seen in Fig. 3(e), (c), and (j). The modified model of S&S is a better approximation than the previous models. However, the accuracy of this model relies strongly on the aspect ratio, and therefore its validity is based upon a detailed knowledge of the microstructure of the reinforcements. Strikingly, the best predictions for particulate reinforcements, where the aspect ratio should not be greater than ~1.5, are obtained for aspect ratio values of $\gtrsim 2$. This is illustrated in Fig. 4,

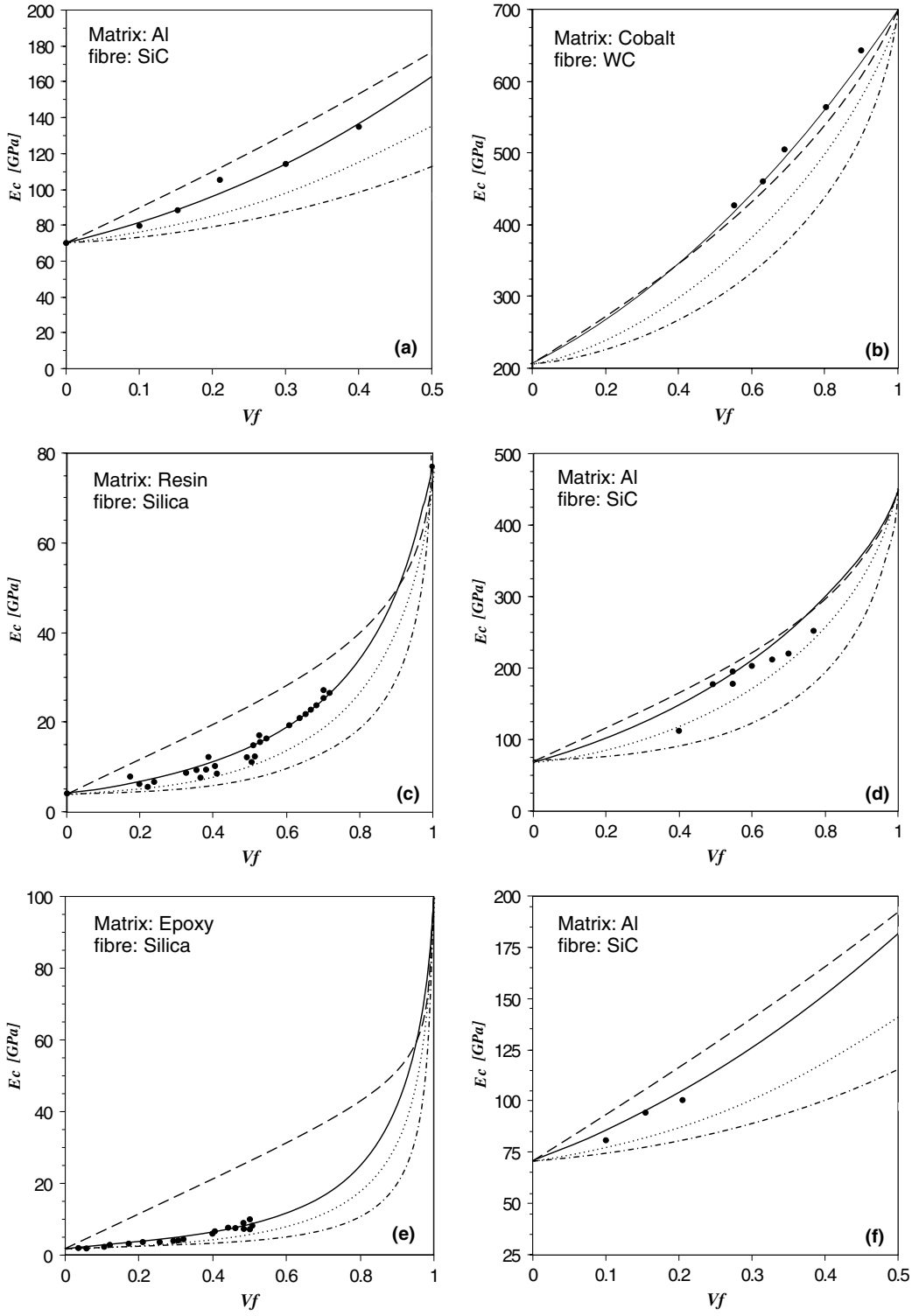

Fig. 3. Experimentally determined Young's moduli of various two-phase composites compared to predicted values using Eq. (6) (solid line). Also included are predictions by equations presented by T&A (dashed-dotted line), R–V–H (dashed line), and S&S (dotted line). Experimental data (black dots) compiled from different sources: a [13]; b, c, d, e, h, i [21]; f [9]; g [15]. Table 2 lists the elastic properties of all phases.

where several experimental data on particulate reinforced Al–SiC composites are plotted together with the predictions from Eq. (6), and R–V–H, T&A, S&S, and Eshelby [20] models. It can be seen that S&S model, using the fibre aspect ratio $s = 1.5$, underpredicts the data by about 15–25% (see also Fig. 6 in S&S), challeng-

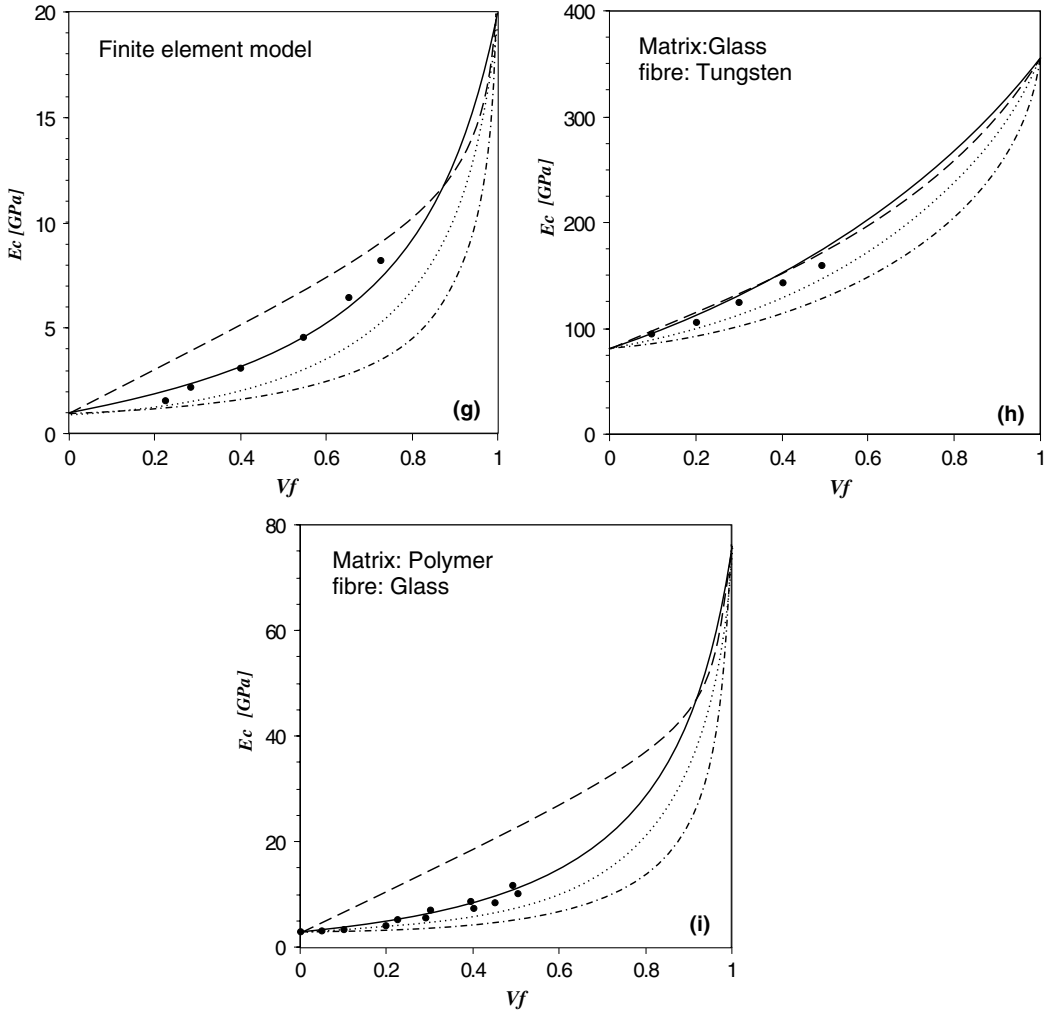

Fig 3. (*continued*)

Table 2
Elastic properties of constituent phases of two-phase composites plotted in Fig. 3

Composite	Matrix	Fibre	E_m (GPa)	E_f (GPa)	V_m	v_f
Al–SiC	Aluminium	SiC	70	450	0.34	0.22
WC–Co	Cobalt	WC	207	700	0.31	0.19
Dental composite	Resin	Silica	4	77.2	0.35	0.25
Epoxy–silica	Epoxy	Silica	2.1	94	0.4	0.25
Glass–tungsten	Glass	Tungsten	81	355	0.2	0.24
Polymer–glass	Polymer	Glass	1.69	70.3	0.44	0.21
FEM	–	–	1	20	0.3	0.3

See caption in Fig. 3 for references.

ing its applicability as a general method. Eq. (6) still gives the best predictions (similar to those by Eshelby model) in all cases, even when other common methods fail.

2.2. Three-phase composites

This section is devoted to derive simple analytical expressions for the elastic properties of three-phase composites based on the shear-lag model discussed in the previous section. A fundamental assumption behind any model for heterogeneous composites is that their heterogeneities can be "homogenized" by choosing a correct *representative volume element* (RVE). This RVE should take into account the mechanical interaction between the phases and maintain accurate volumetric relations. Our preferred microstructural idealization of a three-phase composite is represented in Fig. 5.

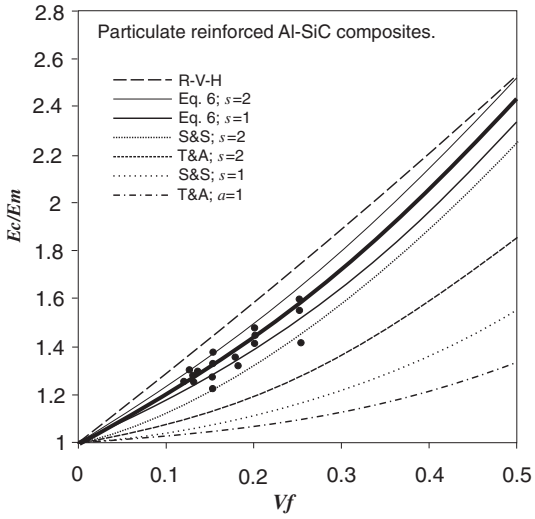

Fig. 4. Comparison of predicted and experimentally determined Young's moduli of particulate reinforced Al–SiC composites, using various models. Eq. (6) with $s = 1.5$ (thick solid line) gives the best predictions, almost identical to those by Eshelby model, not included in the figure for clarity.

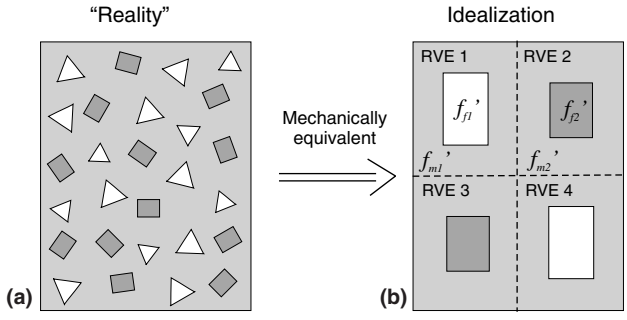

Fig. 5. Scheme of a "real" three-phase composite (a) and of the mechanical equivalent (b) used to calculate Young's modulus of a three-phase composite.

The "real" composite (Fig. 5(a)) is viewed as a combination of several particles of different shapes and sizes, immersed in an isotropic, homogeneous matrix. The idealization (Fig. 5(b)) of the "real" structure is envisaged as four RVE, each containing one fibre that represents the sum of the volumes of the reinforcements of one single phase divided by two. The fibres in these RVE account for the integrated mechanical interaction of many single particles (i.e. reinforcements) in the "real" composite. The choice of this particular configuration of four RVE is justified since it is suitable to assume that, on average, the composite will contain grains that interact mechanically as elements in series and in parallel at the same time. Therefore, we must take into account these two mechanisms in describing the final Young's modulus of the composite. The volume fractions and total volumes of the phases are related by

$$f_i = \frac{V_i}{V_c}, \tag{7}$$

where f_i and V_i are the volume fraction and total volume of the i-phase, respectively. Hence, the following relation holds for a three-phase composite

$$V_c = V_{f1} + V_{f2} + V_m, \tag{8}$$

Referring to Fig. 5, the total volume V'_c in RVE 1 can be expressed as

$$V'_c = \tfrac{1}{4}(V_{f1} + V_{f2} + V_m) \tag{9}$$

and also as

$$V'_c = V'_{f1} + V'_{m1}, \tag{10}$$

where V'_{f1} and V'_{m1} are the new fibre and matrix volumes in RVE 1, respectively. The former is

$$V'_{f1} = \tfrac{1}{2}V_{f1}. \tag{11}$$

Substituting Eq. (11) into (9) and (10) we have

$$V'_{m1} = \tfrac{1}{4}(V_{f2} + V_m - V_{f1}), \tag{12}$$

from which the volume fraction of the matrix in RVE 1 can be obtained as follows:

$$f'_{m1} = \frac{V'_{m1}}{1/4V_c} = f_{f2} + f_m - f_{f1}. \tag{13}$$

Similarly, the volume fraction of the fibre in RVE 1 is

$$f'_{f1} = \frac{1/2V_{f1}}{1/4V_c} = \frac{2V_{f1}}{V_c} = 2f_{f1}. \tag{14}$$

Following the same procedure, the new volume fractions for the fibre and the matrix in the RVE 2 are

$$f'_{m2} = f_{f1} + f_m - f_{f2}, \tag{15}$$

$$f'_{f2} = 2f_{f2}. \tag{16}$$

With these expressions for the volume fractions of the RVE, it is possible to calculate the Young's modulus for each RVE by using Eq. (6). Notice that only two moduli are needed, since the modulus of the RVE 1, E_{c1}, is equal to that of the RVE 4, and the same situation applies for RVE 2 and RVE 3, both of them having modulus E_{c2} (see Fig. 5).

In order to obtain the Young's modulus of the three-phase composite, RVE acting in series (i.e., RVE 1 with RVE 3, and RVE 2 with RVE 4) are considered to undergo isostress, while the two RVE acting in parallel (i.e. RVE 1 + 3 with RVE 2 + 4) are assumed to undergo isostrain load conditions. Similar approaches are used in unit-cell models for two-phase composites (e.g. [21]). The Young's modulus resulting from the combination of RVE 1 and 3 is therefore

$$E_{CA} = \frac{E_{c1}E_{c2}}{E_{c1}f_2 + E_{c2}f_1}, \tag{17}$$

where E_{c1} and E_{c2} are obtained from Eq. (6), and f_1 and f_2 are the volume fractions of each RVE, considered to be the same and equal to 1/2. The elastic modulus of a composite that is loaded in a direction parallel to the interface, assuming the isostrain condition, is known to be $E = E_1 f_1 + E_2 f_2$ [13,21]. Therefore, using Eq. (17) to account for the combination of RVE 1 and 3 (i.e., elements loaded in a direction perpendicular to the interface) into a new single RVE, the final modulus of the three-phase composite can be expressed as

$$E_{CT} = \frac{E_{c1}E_{c2}}{(E_{c1}f_2 + E_{c2}f_1)}(f_1 + f_2) + \frac{E_{c1}E_{c2}}{(E_{c1}f_2 + E_{c2}f_1)}(f_1 + f_2), \tag{18}$$

which, recalling that $(f_1 + f_2)$ is now equal to 1/2, can be simplified to

$$E_{CT} = 2\frac{E_{c1}E_{c2}}{E_{c1} + E_{c2}}. \tag{19}$$

3. Comparison with experimental data

The validity and versatility of our model is tested by comparing predictions with experimentally measured values of various composite materials. However, the scarcity of accurate experimental results precludes a direct assessment, affecting somehow the quality of the comparisons. One potential experimental source comes form acoustic velocities measurements in three-phase natural rocks, since it is one of the most widely used approaches to estimate elastic properties of these materials [12,26]. In doing this, it is important to select only data on three-phase rocks for which the modal composition is known. We assume that Young's modulus E, shear modulus G, Poisson's ratio v, bulk modulus K, and P-wave velocities V_p, can be calculated from elasticity relationships for isotropic and homogeneous materials [22, p. 104]. The Poisson's ratio of the composite is calculated with the following formula:

$$v_c = f_{f1}v_{f1} + f_{f2}v_{f2} + f_m v_m. \tag{20}$$

Although Eq. (20) is strictly an expression for the longitudinal Poisson's ratio (see e.g. [13]), since we are using the fibre configuration as an averaging method, there is no a priori obstacle to its use.

Another source of experimental data is measurements in concrete samples. This material is considered to behave as a three-phase composite, due to the presence of an Interfacial Transition Zone (ITZ) around the inclusions in the cement paste (e.g. [23,24]). The geometry of the ITZ might be quite different from that of a fibre composite, and it is still poorly known. However, there is a general agreement that the volume fraction of the ITZ should not be greater than ~0.14. This value is high enough to noticeably affect the properties of the concrete [2,24]. A similar situation is found in composites of alumina platelets in a mullite matrix (APM), where a "soft" silica-rich phase surrounds the matrix particles. Also in this case, the microstructure of the material is not well understood, but it was shown that the volume fraction of the soft phase should be restricted to ~0.05–0.2 [25]. Volume fractions larger than the latter value are unrealistic and not supported by microscopic observations.

Considering the above volume fraction values as constraints, we can attempt an indirect validation of the model. Due to the lack of detailed information regarding the precise value of the volume fraction of the "soft" phase in concrete and APM samples, we calculate the theoretical variation of the Young's modulus in the composite as a function of the "soft" phase volume fraction. In our calculations we maintain constant the volume fractions of the inclusions, which are predefined values in the experiments, and vary proportionally the matrix and "soft" phase volume fractions. If our approach is correct, predictions from the model should agree with volumes fractions proposed for these materials.

Fig. 6 shows the predictions for acoustic velocities in three natural rocks as a function of the volume fraction of the most abundant phase (not the matrix). The change in elastic moduli with temperature and pressure needs to be considered for each mineral before using Eqs. (6) and (19). Table 3 lists modal compositions and elastic moduli used in the computations, as well as temperature and confining pressure conditions during measurements. Although there are some intrinsic error sources (assumed isotropy and homogeneity for both monomineralic aggregates and polymineralic composites), it can be seen that our model provides a good estimate of the measured values. In this case, our predictions are similar to those obtained from the R–V–H average method. The absolute error is $\lesssim 2\%$, which lies well within the best predictions associated with other methods [26].

Fig. 7 illustrates the case for an APM composite. The variation of the Young's modulus of the composite is plotted as a function of the volume fraction of the "soft" phase around the matrix particles. The volume fraction of the alumina phase is maintained constant and equal to 0.2, as in the real sample [25]. The moduli of the alumina phase, the mullite matrix, and the silica-rich phase are $E_{Al} = 399.6$ GPa, $E_m = 229.1$ GPa, and $E_s = 82.45$ GPa, respectively. The experimental measurement provided by Ledbetter et al. [25] is also included (222 GPa). Therefore, the projection on the horizontal axis of the intersection of the solid line with the experimental value (black dot in Fig. 7), gives the expected volume fraction of the "soft" phase as predicted by our model. The estimated volume fraction (0.13–0.14), within the experimental error, is in perfect agreement

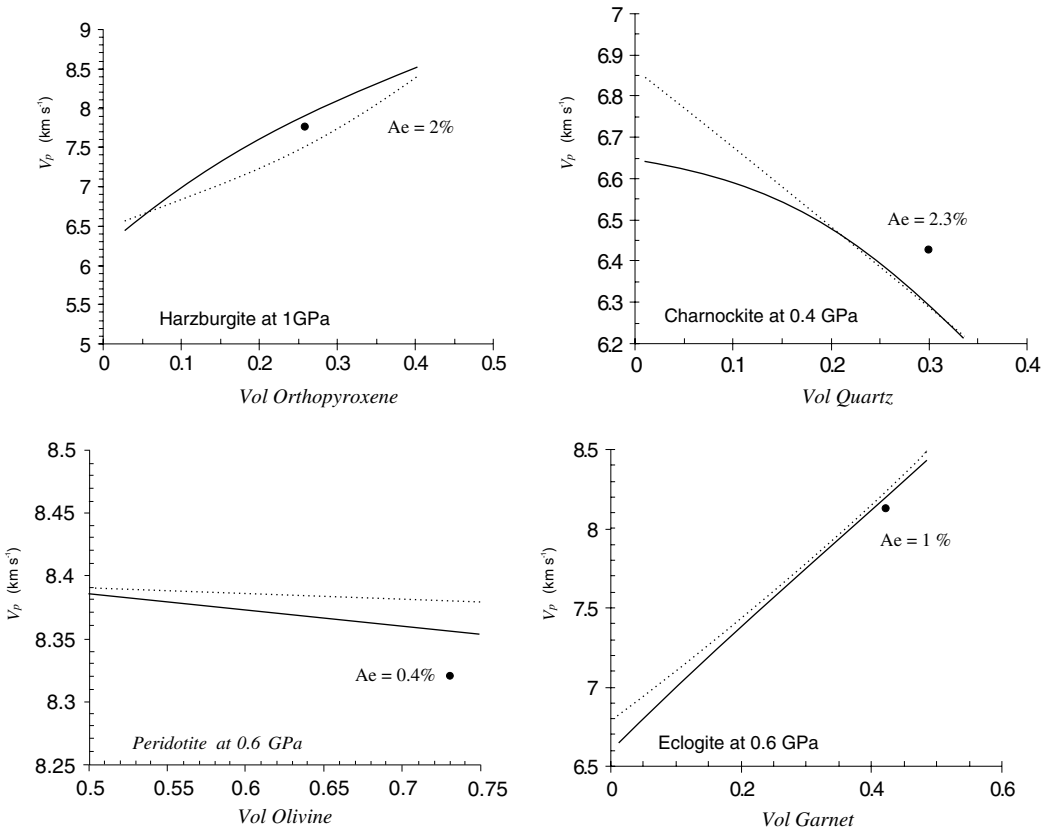

Fig. 6. Comparison of predicted (lines) and measured (black dots) compressional sound velocities in three-phase natural rocks. Solid lines are the predictions from Eqs. (6), (19) and (20). In all cases, the volume fraction of the matrix (i.e., the most abundant phase) is maintained constant. The confining pressures (in GPa) at which velocities were measured are indicated for each sample. Dotted lines are predictions by the R–V–H average method. Ae is the absolute error (%), defined as $\frac{|V_{\text{predicted}}-V_{\text{measured}}|}{V_{\text{measured}}} \times 100$. Modified from [12].

Table 3
Volume fractions, temperature, pressure, and Young's moduli E used in Eqs. (6) and (19) for the four tested rocks

Rock	Temperature (°C)	Pressure (GPa)	Composition	E (GPa)[a]	Reference
Harzburgite BD1675	25.0	1.0	Olivine (60%) Orthopyroxene (24%) Serpentine (16%)	201.22 187.4 43.2[b]	[29]
Charnockite A2	25.0	0.4	Feldespar (64%) Quartz (30%) Orthopyroxene (6%)	69.9 95.56 182.7	[29]
Eclogite XG 98-15	25.0	0.6	Clinopyroxene (50%) Garnet (42%) Mica (8%)	172 243 90	[29]
Peridotite S1-S3-S32	25.0	0.6	Olivine (73%) Orthopyroxene (21%) Clinopyroxene (6%)	197.2 187.2 167	[29]

[a] Calculated from data in [30].
[b] Calculated from [31].

with the values given by Ledbetter et al. [25]. In this case, there is almost no distinction between the predictions of the R–V–H average method and our model. This is due to the relatively small $E_{\text{Al}}/E_{\text{m}}$ ratio, which makes the Reuss and Voigt bounds to be close to each other and to vary almost linearly.

Fig. 8 shows the predictions (solid lines) of the Young's modulus of the composite as a function of the ITZ volume fraction for the case of concrete samples. The moduli of the cement paste and the aggregate (sand) are $E_{\text{cem}} = 20.76$ GPa, and $E_{\text{ag}} = 80$ GPa, respectively. For the ITZ, a typical value of 0.45 E_{cem} is assumed

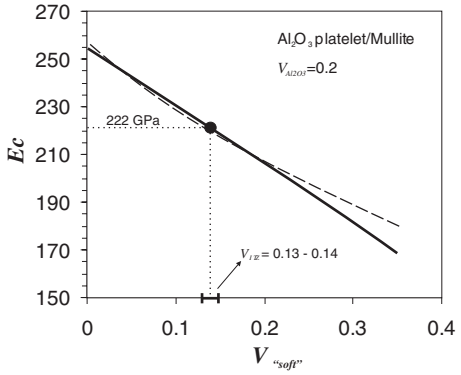

Fig. 7. Variation of Young's modulus of a composite of alumina platelets in a mullite matrix as a function of the "soft" surrounding phase volume fraction. The solid line represents predictions from Eqs. (6) and (19). Dashed line represents predictions by the R–V–H method. The black dot is the intersection between the experimental measurement and theoretical estimation. See text for details.

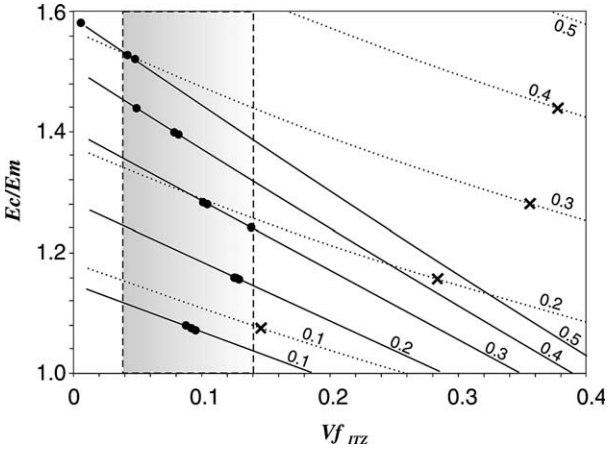

Fig. 8. Comparison of predicted and measured Young's moduli in concrete samples as a function of the ITZ volume fraction. Solid lines are predictions from Eqs. (6) and (19). Dotted lines are predictions by the R–V–H method. Black dots represent the intersection between measured values and theoretical predictions by our model. The projection on the horizontal axis gives the expected volume fraction for the ITZ. The projection of the crosses on the horizontal axis gives the predictions of the R–V–H method. See text for details.

[23,27]. The numbers on each curve of Fig. 8 show the volume fraction of the main phase (i.e. aggregate). Experimental results reported by Yang [23] are also included (black dots). Again, the projection of the intersection between the measured values and the curves gives the theoretical value for the volume fraction of the ITZ. All predicted values lie in the range of 0.01–0.14, and with the exception of only one point, all of them are restricted to the expected range of 0.04–0.14 (grey area in Fig. 8). The variation pattern is also interesting, and some qualitative conclusions can be drawn. The figure shows that a general increase in the theoretical ITZ volume fraction is experienced from low aggregate volume fraction values to moderate values (approximately 0.3). Once the aggregate has reached volume fractions of ~0.3, there is a clear decrease in the ITZ volume fraction, reaching values close to 0 for aggregate volume fractions of 0.5. This indicates that, although the general effect is to harden the composite (i.e., the ratio E_c/E_m always increases), there is a relative elastic softening in the composite for low aggregate volume fractions. In other words, the effect of the third phase is more significant at aggregate volume fractions <0.3, making the hardening effect inferior than that expected from the addition of reinforcement. Once a critical value (~0.3) has been reached, the effect of the reinforcement is more important than that of the ITZ and a general hardening is expected. In this case, predictions from R–V–H average method are well above the expected values (crosses in Fig. 8). Overestimations in ITZ volume fractions are grater for large values of aggregate volume fractions, reaching absolute errors of ~300%.

4. Conclusions

We have presented a new model to calculate the elastic properties of three-phase composites on the basis of a combination of the modified shear-lag model and the unit cell method. Simple analytical expressions are obtained for predicting Young's moduli of polycrystalline/polymineralic three-phase composites. The model only requires knowledge of Young's moduli and volume fractions of the three phases, from which the composite modulus is obtained in a straightforward manner. Neither semiempirical constants nor detailed microstructural information are needed. The model has the potential to include anisotropy effects by means of the aspect ratio s. However, its dependency on s is not as critical as in other models (e.g. S&S, T&A), which tend to give unrealistic estimations of Young's modulus, especially for low s values. These features make the model able to be used as a general method to predict elastic properties of composites having different matrix-reinforcements geometries. The versatility and reliability of the model has been tested on many different materials (concrete, alumina–mullite composites, natural polycrystalline rocks). Predictions are always in good agreement with experimental data found in the literature. This is encouraging for applying the model to other types of three-phase composites, like fibre-reinforced polymers and graphite/fibre epoxy reinforced composites.

Acknowledgements

This work was supported by Carleton University and OGS (Ontario Graduate Scholarship) scholarships to

JCA, and an NSERC (Natural Sciences and Engineering Research Council of Canada) discovery grant to GR. We thank the reviewers for helpful comments on an early version of this paper.

Appendix A

Force equilibrium in the system (Fig. 1) requires that (symbols in Table 1)

$$2\int_0^{r_1} r\sigma_f(x)\mathrm{d}r + 2\int_{r_1}^{R} r\sigma_m(x,r)\mathrm{d}r = R^2\sigma_a, \tag{A.1}$$

$$\frac{\mathrm{d}\sigma_f(x)}{\mathrm{d}x} = -\frac{2\tau(r_1,x)}{r_1}, \tag{A.2}$$

$$r\frac{\partial\sigma_m(x,r)}{\partial x} + r\frac{\partial\tau(x,r)}{\partial r} = -\tau(x,r), \tag{A.3}$$

$$2\pi r_1\tau(r_1,x) = 2\pi r\tau(r,x), \tag{A.4}$$

where $\tau(r,x)$ and $\sigma_m(x,r)$ are, respectively, the shear and axial stress in the matrix.

The governing differential equation for the system in Fig. 1 can be written as [7]

$$\frac{\mathrm{d}^2\sigma_f(x)}{\mathrm{d}x^2} = \frac{\sigma_f(x)HS}{E_fR^2} - H\sigma_a, \tag{A.5}$$

where

$$H = \frac{R^2}{r_1^2(1+v_m)\left[R^2\ln(R/r_1) - \frac{(R^2-r_1^2)}{2}\right]} \tag{A.6}$$

and

$$S = r_1^2E_f + (R^2-r_1^2)E_m. \tag{A.7}$$

The general solution of Eq. (A.13) is of the form $\sigma_f(x) = \sigma_{fH}(x) + \sigma_{fP}(x)$, where $\sigma_{fH}(x)$ is the solution of the homogeneous part and $\sigma_{fP}(x)$ is the solution of the non-homogeneous part (e.g. [28]). It can be proven that such a solution can be written as

$$\sigma_f(x) = \frac{R^2E_f\sigma_a}{S} + C_1\cosh(\beta x) + C_2\sinh(\beta x), \tag{A.8}$$

where

$$\beta = \sqrt{\frac{SH}{R^2E_f}}. \tag{A.9}$$

The two constants C_1 and C_2 are determined by applying appropriate boundary conditions. Similarly, from Eqs. (A.2) and (A.8) we find

$$\tau_f(r_1,x) = -\frac{r_1\beta}{2}[C_2\cosh(\beta x) + C_1\sinh(\beta x)]. \tag{A.10}$$

Applying the following boundary conditions:

$$\begin{aligned}&\sigma_{ff}(L) = \sigma_a; \quad \sigma_f(l) = \sigma_{ff}(l);\\ &\tau_f(r_1,l) = \tau_{ff}(r_1,l); \quad \tau_f(r_1,0) = 0\end{aligned} \tag{A.11}$$

and using Eqs. (A.8)–(A.10) and (3)–(5), we find the values for the constants C_1 and C_2

$$C_1 = 2\frac{\frac{\sigma_a(R^2-r_1^2)(E_m-E_f)}{S}}{\left\langle 2\cosh(\beta l) - \frac{\beta\{2\sinh(\beta l)[\exp(\beta_f l)-\exp[\beta_f(2L-l)]]\}}{\beta_f\{\exp(\beta_f l)+\exp[\beta_f(2L-l)]\}}\right\rangle} = 2A, \tag{A.12}$$

$$C_2 = 0, \tag{A.13}$$

which allows us to rewrite Eqs. (A.8) and (A.10) in the form of Eqs. (1) and (2). Following the same procedure with Eqs. (3) and (4) we get (see also [7])

$$c_1 = \frac{\beta C_1\sinh(\beta l)}{\beta_f\{\exp(\beta_f l) + \exp[\beta_f(2L-l)]\}}, \tag{A.14}$$

$$c_2 = -c_1\exp(2\beta_f L). \tag{A.15}$$

Appendix B

The Young's modulus of the composite can be independently derived from Eqs. (1)–(5) and (A.6)–(A.15) following two different approaches: (a) using average stresses and strains, or (b) using average displacements.

(a) The fundamental equation describing the modulus of the composite can be written as (e.g. [6])

$$E_c = \frac{(1-f_f)\overline{\sigma_m} + f_f\overline{\sigma_f}}{\overline{\varepsilon}_{c(a)}}, \tag{B.1}$$

where $\overline{\varepsilon}_{c(a)}$ is the average strain of the composite, $\overline{\sigma_m}$ is the average stress in the matrix, $\overline{\sigma_f}$ is the average stress in the fibre, and f_f is the volume fraction of the fibre. The average strain is defined as

$$\overline{\varepsilon}_{c(a)} = f_f\frac{\overline{\sigma_f}}{E_f} + (1-f_f)\frac{\overline{\sigma_m}}{E_m}, \tag{B.2}$$

and the average stresses in both the matrix and fibre can be expressed as

$$\begin{aligned}\overline{\sigma_m} = &\left\{2\pi\left\langle\left(\int_0^l\int_{r_1}^R r\sigma_m(x,r) + \int_l^L\int_0^{r_1} r\sigma_{ff}(x)\right.\right.\right.\\ &\left.\left.\left.+\int_l^L\int_{r_1}^R r\sigma_m(x,r)\right)\mathrm{d}r\,\mathrm{d}x\right\rangle\right\}\\ &\Big/\left\{(L-l)R^2\pi + l\pi(R^2-r_1^2)\right\},\end{aligned} \tag{B.3}$$

$$\overline{\sigma_f} = \frac{2\pi}{\pi r_1^2 l}\int_0^l\int_0^{r_1} r\sigma_f(x)\mathrm{d}r\,\mathrm{d}x. \tag{B.4}$$

The function $\sigma_m(x,r)$ in Eq. (B.3) describes the variation of the stress in the matrix. However, there is no need to know the explicit form of this function, since it can be

eliminated by using the equilibrium condition expressed in Eq. (A.1). The combination of Eqs. (A.1) and (B.3) yields

$$\overline{\sigma_{\mathrm{m}}} = \left\{ 2\pi \left\langle \int_0^l \left(\frac{R^2\sigma_{\mathrm{a}}}{2} - \int_0^{r_1} r\sigma_{\mathrm{f}}(x)\mathrm{d}r \right)\mathrm{d}x + \int_l^L \int_0^{r_1} r\sigma_{\mathrm{ff}}(x)\mathrm{d}r\,\mathrm{d}x + \int_l^L \left(\frac{R^2\sigma_{\mathrm{a}}}{2} - \int_0^{r_1} r\sigma_f(x)\mathrm{d}r \right)\mathrm{d}x \right\rangle \right\} \Big/ \left\{ (L-l)R^2\pi + l\pi(R^2 - r_1^2) \right\}. \quad \text{(B.5)}$$

Finally, combining Eqs. (B.2), (B.4) and (B.5), and substituting into Eq. (B.1), the Young's modulus of the composite can be calculated.

(b) The fundamental equation in this approach is the usual relation

$$E_{\mathrm{c}} = \frac{\sigma_{\mathrm{a}}}{\overline{\varepsilon_{\mathrm{c(b)}}}}, \quad \text{(B.6)}$$

where $\overline{\varepsilon_{\mathrm{c(b)}}}$ is the average strain of the composite, expressed as

$$\overline{\varepsilon_{\mathrm{c(b)}}} = \frac{d_0}{L}, \quad \text{(B.7)}$$

where L is the length of the unit cell (see Fig. 1) and d_0 is the average displacement at $x = L$. The value of L and R as a function of the volume fraction of the fibre is calculated as [15]

$$L = l f_{\mathrm{f}}^{2p-1}; \quad R = r/f_{\mathrm{f}}^{-p}; \quad p = \frac{1}{2} - \frac{1}{6}\exp\left(\frac{-l}{5r_1}\right). \quad \text{(B.8)}$$

The total average displacement of the unit cell d_0 can be expressed as

$$d_0 = \frac{2}{R^2}\left(\int_0^l \int_0^{r_1} r\frac{\sigma_{\mathrm{f}}(x)}{E_{\mathrm{f}}} + \int_0^l \int_{r_1}^R r\frac{\sigma_{\mathrm{m}}(x,r)}{E_{\mathrm{m}}} \right)\mathrm{d}r\,\mathrm{d}x + \frac{(L-l)\sigma_{\mathrm{a}}}{E_{\mathrm{m}}}, \quad \text{(B.9)}$$

which, after solving the integrals and rearranging, gives the average strain of the composite as

$$\overline{\varepsilon_{\mathrm{c(b)}}} = \frac{\sigma_{\mathrm{a}}}{E_{\mathrm{m}}} + \left[\left(\frac{2A\sinh(\beta l)}{\beta} + \frac{lR^2E_{\mathrm{f}}\sigma_{\mathrm{a}}}{S} \right) \times \left(\frac{1}{E_{\mathrm{f}}} - \frac{1}{E_{\mathrm{m}}} \right) \frac{r_1^2}{LR^2} \right]. \quad \text{(B.10)}$$

Again, the explicit formulation of the stress in the matrix $\sigma_{\mathrm{m}}(x,r)$ is not required in solving Eq. (B.9). Therefore, substituting Eq. (B.10) into Eq. (B.6), we finally obtain the expression for the Young's modulus of the composite as in Eq. (6).

References

[1] Nilsen AU, Monteiro PJM. Concrete: a three phase material. Cement Concrete Res 1993;23:147–51.

[2] Metha PK, Monteiro PJM. Concrete: structure, properties, and methods. 2nd ed. Englewood Cliffs (NJ): Prentice-Hall; 1993.

[3] Kim P. A comparative study of the mechanical performance and cost of metal, FRP and hybrid beams. Appl Compos Mater 1998;5:175–87.

[4] Palumbo M, Tempesti E. Fiber-reinforced syntactic foams as a new lightweight structural three-phase composite. Appl Compos Mater 2001;8:343–59.

[5] Cox HL. The elasticity and strength of paper and other fibrous materials. Br J Appl Phys 1952;3:72–9.

[6] Nair SV, Kim HG. Modification of the shear lag analysis for determination of elastic modulus of short-fiber (or Whisker) reinforced metal matrix composites. J Appl Mech 1992;59:176–82.

[7] Hsueh C-H. A modified analysis for stress transfer in fibre-reinforced composites with bonded fibre ends. J Mater Sci 1995;30:219–24.

[8] Beyerlein IJ, Landis CM. Shear-lag model for failure simulations of unidirectional fiber composites including matrix stiffness. Mech Mater 1999;31:331–50.

[9] Starink MJ, Syngellakis S. Shear lag models for discontinuous composites: fibre end stresses and weak interface layers. Mater Sci Eng 1999;A270:270–7.

[10] Nardone VC, Prewo KM. On the strength of discontinuous silicon carbide reinforced aluminum composites. Scripta Metall Mater 1986;20:43–8.

[11] Clyne TW. A simple development of the shear lag theory appropriate for composites with a relatively small modulus mismatch. Mater Sci Eng 1989;A122:183–92.

[12] Afonso JC, Ranalli G, Fernàndez M. Thermal expansivity and elastic properties of the lithospheric mantle: results from mineral physics of composites. Phys Earth Planet Int 2005 [in press].

[13] Hull D, Clyne TW. An introduction to composite materials. 2nd ed. UK: Cambridge University Press; 1996. p. 326.

[14] Zhao P, Ji S. Refinements of the shear-lag model and its applications. Tectonophysics 1997;279:37–53.

[15] Hsueh C-H. Young's modulus of unidirectional discontinuous-fibre composites. Compos Sci Technol 2000;60:2671–80.

[16] Nardone VC. Assessment of models used to predict the strength of discontinues silicon carbide reinforced aluminium alloys. Scripta Metall 1987;21:1313–8.

[17] Taya M, Arsenault RJ. Metal matrix composites: thermomechanical behavior. Oxford: Pergamon Press; 1989.

[18] Levy A, Papazian JM. Tensile properties of short fibre-reinforced SiC/Al composites: part II. Finite element analysis. Metall Trans 1990;21A:411–20.

[19] Hill R. The elastic behavior of a crystalline aggregate. Proc Roy Soc London Serial 1952;A65:349–54.

[20] Eshelby JD. The elastic field outside an ellipsoidal inclusion. Proc Roy Soc London 1959;A252:561–9.

[21] Ravichandran KS. Elastic properties of two-phase composites. J Am Ceram Soc 1994;77(5):1178–84.

[22] Jaeger JC, Cook NGW. Fundamentals of rock mechanics. London: Methuen & Co Ltd; 1969.

[23] Yang CC. Effect of the transition zone on the elastic moduli of mortar. Cement Concrete Res 1998;28:727–36.

[24] Li G, Zhao Y, Pang S-S. Four-phase sphere modeling of effective bulk modulus of concrete. Cement Concrete Res 1999;29:839–45.

[25] Ledbetter H, Kim S, Dunn M, Xu Z, Crudele S, Kriven W. Elastic constants of mullite containing alumina platelets. J Eur Ceram Soc 2001;21:2569–76.

[26] Ji S, Wang Q, Xia B. *P*-wave velocities of polymineralic rocks: comparison of theory and experiment and test of elastic mixture rules. Tectonophysics 2003;366:165–85.
[27] Lutz MP, Monteiro PJM, Zimmerman RW. Inhomogeneous interfacial transition zone model for the bulk modulus of mortar. Cement Concrete Res 1997;27:1113–22.
[28] Kreyszig E. Advanced engineering mathematics. NY: John Wiley & Sons; 1988.
[29] Ji S, Wang Q, Xia B. Handbook of seismic properties of minerals, rocks and ores. Montreal: Polytechnic Int. Press; 2002.
[30] Bass JD. Elasticity of minerals, glasses, and melts. In: Ahrens TJ, editors. Mineral physics & crystallography – a handbook of physical constants, vol. 2. AGU Reference Shelf. p. 45–63.
[31] Christensen NI. Compressional wave velocities in rocks at high temperature and pressures, critical thermal gradients, and crustal low-velocity zones. J Geophys Res 1979;84:6849–57.